Mon. Not. R. Astron. Soc. **000**, 1–?? (2002) Printed 11 January 2013 (MN LATEX style file v2.2)

Atmospheric Parameters of 169 F, G, K and M-type Stars in the *Kepler* Field*

J. Molenda-Żakowicz[1], S.G. Sousa[2], A. Frasca[3], K. Uytterhoeven[4,5,6], M. Briquet[7,8], H. Van Winckel[8], D. Drobek[1], E. Niemczura[1], P. Lampens[9], J. Lykke[10], S. Bloemen[8], J.F. Gameiro[2], C. Jean[8], D. Volpi[9], N. Gorlova[8], A. Mortier[2,11], M. Tsantaki[2,11], G. Raskin[8]

[1] *Instytut Astronomiczny Uniwersytetu Wrocławskiego, ul. Kopernika 11, 51-622 Wrocław, Poland, E-mail: molenda@astro.uni.wroc.pl*
[2] *Centro de Astrofísica, Universidade do Porto, Rua das Estrelas, 4150-762 Porto, Portugal*
[3] *INAF, Osservatorio Astrofisico di Catania, via S. Sofia, 78, 95123 Catania, Italy*
[4] *Kiepenheuer-Institut für Sonnenphysik, Schöneckstr. 6, D-79104 Freiburg, Germany*
[5] *Instituto de Astrofísica de Canarias, 38200 La Laguna, Tenerife, Spain*
[6] *Departamento de Astrofísica, Universidad de La Laguna, 38205 La Laguna, Tenerife, Spain*
[7] *Institut d'Astrophysique et de Géophysique, Université de Liège, Allée du 6 Août 17, Bât B5c, 4000 Liége, Belgium*
[8] *Instituut voor Sterrenkunde, KU Leuven, Celestijnenlaan 200D, 3001 Leuven, Belgium*
[9] *Koninklijke Sterrenwacht van België, Ringlaan 3, 1180 Brussel, Belgium*
[10] *Nordic Optical Telescope, 38700 Santa Cruz de La Palma, Spain*
[11] *Departamento de Física e Astronomia, Faculdade de Ciências, Universidade do Porto, Portugal*

Accepted 1988 December 15. Received 1988 December 14; in original form 1988 October 11

ABSTRACT

Both the asteroseismic and planetary studies need precise and accurate atmospheric parameters of the stars as input. We aim at deriving the effective temperature ($T_{\rm eff}$), the surface gravity ($\log g$), the metallicity ([Fe/H]), the projected rotational velocity ($v \sin i$) and the MK type for 169 F, G, K, and M-type *Kepler* targets which were observed spectroscopically from the ground with five different instruments. We use two different spectroscopic methods to analyse 189 high-resolution, high-signal-to-noise spectra acquired for those 169 stars. For 69, $T_{\rm eff}$, $\log g$, [Fe/H], $v \sin i$, and the MK type are derived for the first time. KIC 9025370, 9693187 and 11179629 are discovered to be double-lined spectroscopic binary systems. The results obtained for those stars for which independent determinations of the atmospheric parameters are available in the literature are used for a comparative analysis. As a result, we show that for the solar-type stars the accuracy of the present determinations of $T_{\rm eff}$ is ± 150 K, ± 0.15 dex in [Fe/H], and ± 0.3 dex in $\log g$. Finally, we confirm that the analysis of the curve-of-growth and the method of the spectral synthesis yield systematically different results when they are applied to stars of $T_{\rm eff}$ ranging from 6,000 to 7,000 K.

Key words: stars: atmospheric parameters – space missions: *Kepler*

* Based on observations acquired at the Canada-France-Hawaii Telescope (CFHT) which is operated by the National Research Council of Canada, the Institut National des Sciences de l'Univers of the Centre National de la Recherche Scientifique of France, and the University of Hawaii, the Telescope Bernard Lyot (USR5026) operated by the Observatoire Midi-Pyrénées (Université de Toulouse and the Institut National des Science de l'Univers of the Centre National de la Recherche Scientifique of France), the Nordic Optical Telescope, operated jointly by Denmark, Finland, Iceland, Norway, and Sweden, and with the Mercator telescope, operated by the Flemish Community, both located on the island of La Palma at the Spanish Observatorio del Roque de los Muchachos of the Instituto de Astrofísica de Canarias, and the M.G. Fracastoro station of the INAF - Osservatorio Astrofisico di Catania, Italy. The Mercator observations were obtained with the HERMES spectrograph, which is supported by the Fund for Scientific Research of Flanders (FWO), Belgium, the Research Council of K.U.Leuven, Belgium, the Fonds National de la Recherche Scientifique (FNRS), Belgium, the Royal Observatory of Belgium,

1 INTRODUCTION

Since March 2009, the 105 $\deg^2$ field located between the constellations of Cygnus and Lyra has been continuously monitored by the NASA space mission *Kepler* (Borucki et al. 2003; Koch et al. 2010). The $T_{\rm eff}$, $\log g$, and [Fe/H] of the stars in the *Kepler* field of view, derived from the Sloan *griz* photometry, are provided in the *Kepler* Input Catalog (KIC, Brown et al. 2011) which was created with the aim of providing the distinction between main-sequence stars and giants in the temperature range from 4,500 to 6,500 K. Within that range, the nominal precision of $T_{\rm eff}$ in the KIC is 200 K and 0.5 dex in $\log g$. Beyond those limits, the $T_{\rm eff}$ and $\log g$ in the KIC become imprecise, while the estimates of [Fe/H] are poor in general (Brown et al. 2011). Therefore, ground-based follow-up observations are essential information because they provide the precise and accurate atmospheric stellar parameters needed for detailed asteroseismic and planetary studies of the *Kepler* targets.

Systematic observations aiming at deriving the atmospheric parameters of stars in the *Kepler* field were started well before the *Kepler* satellite was launched (see Molenda-Żakowicz et al. 2007). After the successful launch of the mission more programmes of ground-based follow-up observations started. Eventually, in the frame of the *Kepler* Asteroseismic Science Consortium[1] (KASC) it has been decided that the most optimal approach to observing *Kepler* stars from the ground should consist of a series of coordinated proposals for spectroscopic and photometric observations (see Uytterhoeven et al. 2010a,b).

In this paper, we report on the results of those observations. In Sect. 2, we outline the method of selecting targets. In Sect. 3, we provide the information about the instruments and the data acquisition, reduction and calibration. Our methods of the analysis are described in Sect. 4. In Sect. 5, the atmospheric parameters are provided and compared with the other determinations reported in the literature. Sect. 6 contains the discussion of the accuracy of our results and the accuracy of the determinations of the atmospheric parameters of the solar-type stars. Sect. 7 provides the summary.

2 TARGET SELECTION

The stars which were observed with the FRESCO spectrograph at the 91-cm telescope at INAF-OACt (the principal investigator: JM-Ż) were selected from those faint ($V > 8$ mag), mid-F ($B - V > 0.5$ mag), close (the parallax $\pi > 20$ mas) stars in the Tycho catalog (Hog et al. 2000) which have optical counterparts of X-ray sources in the ROSAT All-Sky Survey Catalogue (see Guillout et al. 1999). These stars were proposed for *Kepler* asteroseismic targets and for the follow-up ground-based observations by AF in the first call for proposals announced by KASC.

The selection of stars to be observed with the FIES spectrograph at the NOT (the principal investigator: KU) and these for the HERMES spectrograph at the Mercator telescope (the principal investigators: MB and EN) was based on the requests of the KASC community which were submitted by the chairs of seven working groups (WGs): Solar-like p-mode Oscillations (WG 1), Oscillations in Clusters (WG 2), Beta Cephei Stars (WG 3), Delta Scuti stars (WG 4), Slowly Pulsating B-stars (WG 6), Cepheids (WG 7), and Gamma Doradus stars (WG-10). In this paper, we report on those stars which are cooler than 7,000 K. The atmospheric parameters derived for the hotter targets will be published by Niemczura et al. (in prep.) and Catanzaro et al. (in prep.)

Our list of the programme stars includes also these *Kepler* targets which were observed with the ESPaDOnS spectrograph at the Canada-France-Hawaii Telescope and the NARVAL spectrograph at the Bernard Lyot Telescope, and for which the data are now public.

The total number of spectra which we analyse is 189. However, because 15 stars were observed with two instruments and one star, with three, the number of the individual stars discussed in this paper is 169. The stars with multiple observations are used for an internal check of the consistency of our results. Those for which $T_{\rm eff}$, $\log g$, and [Fe/H] have been published by Bruntt et al. (2012) or Thygesen et al. (2012) are included for the sake of analysing possible differences in the results obtained by means of different methods.

3 OBSERVATIONS

Our programme stars were observed with five different instruments. Their names are provided in Table 1 which lists also the names of the telescopes, the acronyms of observatories, the number of acquired spectra (N), the year in which the data were acquired, the spectral range and the resolving power (R) of the spectra, the exposure time, and the typical signal-to-noise ratio (S/N) along with the location in the spectrum where it was measured.

For all the instruments, the bias and the flat field measurements were acquired in the evening and in the morning. The spectra of the calibration lamps were acquired in the same time and occasionally during the night. Only for FIES the calibration lamps were acquired before each science observation. The procedures of the data reduction and calibration included the correction for bias and flat field, extraction of the orders, the wavelength calibration, and the cleaning from the cosmic rays. The normalization of the spectra to the level of unity was done manually with IRAF[2].

3.1 FIES

FIES (FIber-fed Echelle Spectrograph) is a cross-dispersed high-resolution échelle spectrograph mounted on the 2.56-m Nordic Optical Telescope (NOT) at the Observatorio Roque de los Muchachos (ORM) on La Palma, Spain. We used the medium-resolution mode ($R = 46,000$) to observe the bright stars ($V < 10$ mag), and the low-resolution mode ($R =$

the Observatoire de Genève, Switzerland and the Thüringer Landessternwarte Tautenburg, Germany.

[1] http://astro.phys.au.dk/KASC/

[2] IRAF is distributed by the National Optical Astronomy Observatory, which is operated by the Association of Universities for Research in Astronomy, Inc.

Table 1. The summary of the instruments and the observations.

Instrument	Telescope	Observatory	N	Year of observations	Spectral range [Å]	R	$t_{\rm exp}$ [s]	S/N
FIES	NOT	ORM	4	2010-2011	3700-7300	46,000	420-2050	100 at 4900 Å
FIES	NOT	ORM	4	2010-2011	3700-7300	25,000	1500-2600	100 at 4900 Å
FRESCO	91-cm	INAF-OACt	18	2009-2010	4300-6800	21,000	2700-4200	80 at 6500 Å
HERMES	Mercator	ORM	20	2010-2011	3800-9000	85,000	500-2600	90 at 6500 Å
NARVAL	TBL	Pic du Midi	50	2010	3700-10500	75,000	< 900	100 at 5200 Å
ESPaDOnS	CFHT	CFH	91	2010	3700-10500	80,000	< 900	100 at 5200 Å

25, 000), for the faint ($V > 10$ mag). The observations were carried out by EN and JL. The spectra were reduced and calibrated using the dedicated reduction software *FIEStool* (Stempels 2004) that is based on existing standard IRAF reduction procedures.

3.2 FRESCO

FRESCO, now de-commissioned, was a fiber-linked REOSC échelle spectrograph attached to the 91-cm telescope at the INAF - Osservatorio Astrofisico di Catania (INAF-OACt), Italy. The observations were carried out by JM-Ż. The data were reduced and calibrated with IRAF.

3.3 HERMES

HERMES is a fiber-fed échelle spectrograph attached to the Flemish 1.2-m telescope Mercator on La Palma, Canary Islands, Spain. It is optimised for high resolution, stability, and broad wavelength coverage which is achieved primarily by implementing an image slicer, an anti-fringe CCD coating, and a thermal enclosure (Raskin et al. 2011). We used that instrument to observe stars brighter than $V = 10$ mag. The observations were carried out by DD, PL, JG, NG, DV, SB, and CJ. The data reduction and calibration were performed with a dedicated Python-based pipeline (Raskin et al. 2011).

3.4 ESPaDOnS and NARVAL

The ESPaDOnS and the NARVAL spectrographs are very similar instruments. ESPaDOnS is mounted at the 3.6-m Canada-France-Hawaii Telescope in the USA while NARVAL is mounted at the 2-m Bernard Lyot Telescope at the Pic du Midi Observatory in France. Both instruments observed the *Kepler* targets in the service mode. All those data are available at the public archive of the Canada-France-Hawaii Telescope (CFHT) Science Data Archive and the CNRS/INSU CDAB/Bass2000 TBLegacy database. The reduction and calibration of the ESPaDOnS and NARVAL data were performed as part of the service programme by means of the data reduction software Libre-ESpRIT written and provided by J.-F. Donati from IRAP, Observatoire Midi-Pyrénées (Donati et al. 1997).

4 METHODS OF THE ANALYSIS

4.1 ROTFIT

The code ROTFIT which we used for deriving $T_{\rm eff}$, $\log g$, [Fe/H], $v \sin i$, and the MK type of all the 169 stars from our sample was developed by Frasca et al. (2003, 2006). This method is similar to that of Katz et al. (1998) and Soubiran et al. (1998). It consists of comparing the spectra of the programme stars, order by order, with the spectra of the reference stars for which the atmospheric parameters are precisely measured from high-resolution, high-S/N spectra. The MK classification of the target spectrum is inferred by adopting the spectral type and the luminosity class of those reference stars which occur most frequently. For the measure of the agreement of spectra, the value of χ^2 is used. As shown by Frasca et al. (2006), this method allows for simultaneous, fast and accurate determination of $T_{\rm eff}$, $\log g$, [Fe/H], $v \sin i$ and the MK type even from spectra of low signal-to-noise ratio or moderate resolution.

The atmospheric parameters of the programme stars are computed as the weighted means of the astrophysical parameters of the ten reference stars which best reproduce the target spectrum, separately in each order. Therefore, per each order weighted averages and standard errors are computed for each of the atmospheric parameters, so that the values from individual orders can be averaged using $\sigma^{-2}\chi^{-2}f$ for a weight. Here, χ^{-2} accounts for differences between orders due to different S/N and the goodness of the fit, while f is proportional to the total absorption of lines in each individual order. The factor f allows for correction for the different amount of information contained in the blue and the red orders which contain different number of the spectral lines, and it gives more weight to the orders which contain strong and broad lines.

Our library of the reference stars contains 221 high-resolution (R = 42,000), high-S/N spectra of slowly rotating stars acquired with the fiber-fed échelle spectrograph ELODIE at the Haute-Provence Observatory which are available from the ELODIE archive (Prugniel & Soubiran 2001). The atmospheric parameters of most of those stars were adopted from the PASTEL catalogue (Soubiran et al. 2010) which provides a literature compilation of stellar atmospheric parameters derived from high-resolution, high-S/N spectra.

4.2 ARES+MOOG

The spectroscopic stellar parameters ($T_{\rm eff}$, $\log g$, $\xi_{\rm t}$, and [Fe/H]) were derived following the same procedure as that used in the previous works (Santos et al. 2004; Sousa et al. 2006, 2008, 2011a,b). This method is based on the measurement of the equivalent widths (EWs) of the Fe I and Fe II weak absorption lines and then imposing the excitation and the ionization equilibrium assuming the LTE approximation. The 2002 version of the code MOOG (Senden 1973) is used together with the grid of the Kurucz Atlas 9 plane-parallel model atmospheres (Kurucz 1993). In this procedure, [Fe/H] is the proxy of metallicity. The equivalent widths are measured automatically with the ARES code (Automatic Routine for line Equivalent widths in stellar Spectra) by Sousa et al. (2007) which successfully reproduces the common manual, interactive determination of EWs.

Since both ARES and MOOG are the core codes used in this method, we refer to it as to ARES+MOOG. Nevertheless, we would like to emphasise that these two codes do not fully describe this method. One of its unique characteristics is the list of the iron lines. Although a preliminary large list of nearly 500 lines was compiled from the Vienna Atomic Line Database (Kupka et al. 1999), the final list includes nearly 300 lines that were carefully tested when automatically measured with ARES (Sousa et al. 2008). Another important aspect of that list are the adopted atomic parameters for each line: The oscillator strengths ($\log gf$) of the lines were recomputed through an inverse analysis of the Solar spectrum allowing this way to perform a differential analysis relatively to the Sun.

The errors of the parameters derived with ARES+MOOG were obtained by quadratically adding 60 K, 0.1 and 0.04 dex to the method's intrinsic errors in $T_{\rm eff}$, $\log g$, and [Fe/H], respectively. The former values were obtained by measuring the typical standard deviation of the parameters discussed by Sousa et al. (2008). A more complete discussion about the errors derived for this spectroscopic method can be found in Sousa et al. (2011a).

Since we adopt a differential analysis (using the Sun for the reference), this method is expected to work very well for solar-type stars and to be less accurate for the cooler and the hotter stars, and those which are significantly different from the Sun. For this reason, we don't provide results for stars cooler than around 4,500 K. Moreover, since ARES+MOOG requires precise measurements of the EWs, we don't provide results for stars showing $v \sin i > 10$ km s^{-1}, which causes the line blending and consecutive problems for the precise determination of EW, and those observed with a resolving power $R < 25,000$.

5 ATMOSPHERIC PARAMETERS

The parameter $T_{\rm eff}$, $\log g$, [Fe/H], and $v \sin i$ with their standard deviations, and the MK types derived with the ROTFIT code are listed in columns 2-10 of Table 2. The $T_{\rm eff}$, $\log g$, [Fe/H], and $\xi_{\rm t}$ with their standard deviations derived with ARES+MOOG are listed in columns 11-18. The KIC numbers of the stars are provided in the first column and the names of the instrument, in the last. We use bold font for the KIC numbers of these stars for which the atmospheric parameters are derived for the first time. Whenever an instrument name is written in bold font, it indicates that the respective spectrum is first analysed in this paper.

Table 2 does not include KIC 9025370, 9693187 and 11179629 which we detect lines of both components in the spectrum. We classify those stars as double-lined spectroscopic binaries (SB2) and do not compute for them the atmospheric parameters.

For KIC 6370489, 10709834, and 10923629 we do not provide the atmospheric parameters obtained with ARES+MOOG. In the spectrum of the first star we find too few useful spectral lines for ARES+MOOG to converge. For KIC 10709834 and 10923629, ARES+MOOG yields very high $\log g$ which are not confirmed with ROTFIT. Therefore, we suspect that the results produced by ARES+MOOG for those two stars may be spurious.

Below, we discuss the $T_{\rm eff}$, $\log g$, and [Fe/H] computed with ARES+MOOG and with ROTFIT. We compare these results with each other and with those obtained by Bruntt et al. (2012) and Thygesen et al. (2012) with the VWA code. We show also how our determinations confront with the temperatures derived with the infra-red flux method (IRFM) by Pinsonneault et al. (2012).

5.1 Effective temperature

As shown in Fig. 1, the differences between $T_{\rm eff}$ derived with ARES+MOOG, ROTFIT, VWA and IRFM show standard deviation ranging from 97 to 179 K, different offsets and trends. The standard deviation is lowest but still significant when the comparisons concern $T_{\rm eff}$ computed with VWA (Fig. 1 *b*, *d*, and *f*). This must be related to the fact that VWA was applied to high-S/N, high-resolution spectra from ESPaDOnS and NARVAL: When the data of high quality are used, all methods yield $T_{\rm eff}$ which are more precise, accurate, and consistent with each other.

For stars with $T_{\rm eff} > 6,000$ K, the effective temperatures derived with ARES+MOOG are systematically hotter then those obtained either with ROTFIT or with VWA (Fig. 1 *a* and *b*.) Between 5,000 K and 6,000 K these three methods agree well but for stars cooler than 5,000 K, ARES+MOOG yields slightly higher $T_{\rm eff}$ which is why for the coolest stars the agreement between ARES+MOOG and ROTFIT or VWA is worse again. The reason for this may be related with the selection of the spectral lines. The original list of lines was optimized for solar-type stars. For cool stars, many of those lines are affected by blending. This effect contributes strongly for the observed offset in temperature. A refinement of the selection of the lines to produce consistent results in this temperature regime will be presented by Tsantaki et al. 2013 (in prep.).

Fig. 1 *a* and *b* show that when ROTFIT and VWA are compared to ARES+MOOG, the differences show similar pattern. This suggest that $T_{\rm eff}$ obtained with ROTFIT and VWA should be close to each other. Indeed, the mean difference between $T_{\rm eff}$ derived by means of those two methods is relatively low, only 70 K. Nevertheless, the standard deviation of the differences between them, 123 K, is still quite high (Fig. 1 *d*.)

When compared with the IRFM-based $T_{\rm eff}$ measured by Pinsonneault et al. (2012), the $T_{\rm eff}$ derived with ARES+MOOG show a negligible offset of 7 K but still a

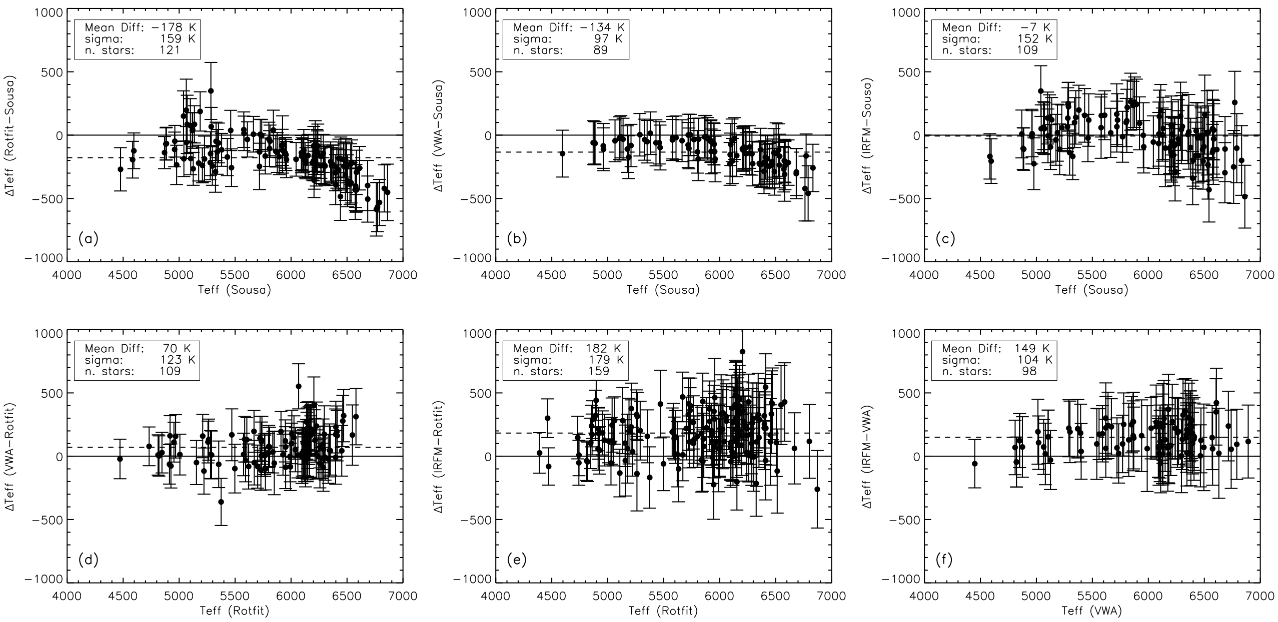

Figure 1. Comparison of the $T_{\rm eff}$ measured with ROTFIT and ARES+MOOG with each other, and with the $T_{\rm eff}$ obtained with VWA by Bruntt et al. (2012) and Thygesen et al. (2012). The $T_{\rm eff}$ obtained by means of each of these three methods are compared also to the IRFM $T_{\rm eff}$ reported by Pinsonneault et al. (2012). In the insets, we give the mean difference between the compared sets of data, the standard deviation of the mean, and the number of stars in common. For the clarity of the plot, the method ARES+MOOG is abbreviated to 'Sousa'.

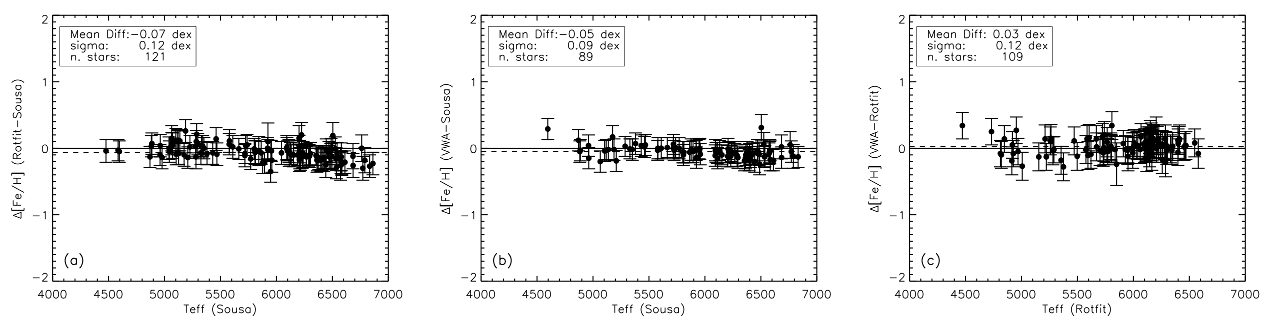

Figure 2. Comparison of the [Fe/H] measured with ROTFIT and ARES+MOOG with each other, and with the spectroscopic [Fe/H] obtained with VWA by Bruntt et al. (2012) and Thygesen et al. (2012). In the insets, we give the mean difference between the compared sets of data, the standard deviation of the mean, and the number of stars in common. For the clarity of the plot, the method ARES+MOOG is abbreviated to 'Sousa'.

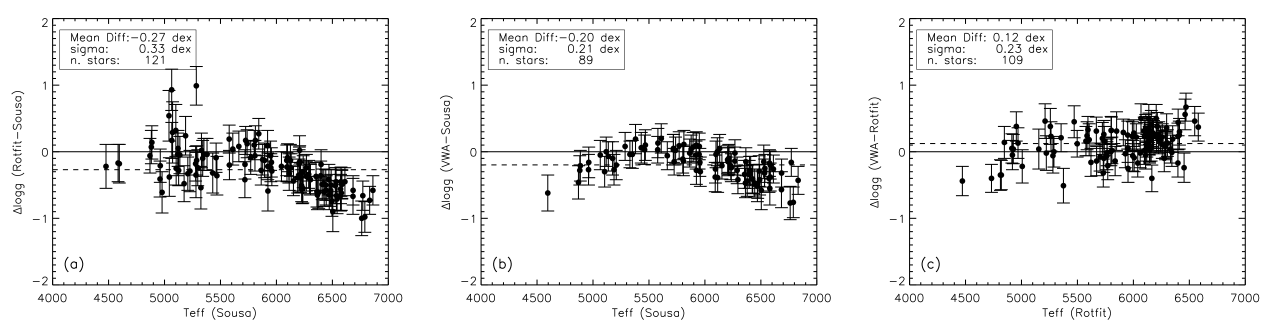

Figure 3. The same as in Fig. 2 but for $\log g$.

high standard deviation of 152 K (Fig. 1 *c*). The two other methods, ROTFIT and VWA, show a much higher mean difference, 182 and 149 K, and a similar standard deviation, 179 and 104 K, respectively (Fig. 1 *e* and *f*). Therefore, it is difficult to say which of those methods, if any, agrees with IRFM best.

Since ARES+MOOG is known to be in a very good agreement with the IRFM scale of temperatures (see Sousa et al. 2008), we expected the results shown in Fig. 1 *c* to compare much better. One of the plausible explanations of the observed scatter is the fact that the IRFM-based $T_{\rm eff}$ provided by Pinsonneault et al. (2012) were derived only from one colour index, $(J-K_S)$, and as such are offset from the conventional IRFM temperature scale (see Figs. 9 and 13, and the discussion in Section 3.3 in Pinsonneault et al. 2012). When Fig. 13 in Pinsonneault et al. (2012) is compared to our Fig. 1 *c*, one can see that the trends and the scatter in both figures are similar. We find it to be a confirmation that $T_{\rm eff}$ derived with ARES+MOOG and IRFM are consistent, and that the high standard deviation of the results shown in Fig. 1 *c* is specific to the properties of $(J-K_S)$ colour index, not due to the imperfection of ARES+MOOG.

One should also keep in mind that the IRFM $T_{\rm eff}$ derived by Pinsonneault et al. (2012) may be to some extent affected by the reddening of the stars. These authors do correct the observed magnitudes for the interstellar extinction, however, since there are no individual measurements of $E(B-V)$ for each target, they use the map-based estimates of extinction from the KIC. Those values are not accurate as has been shown by Molenda-Żakowicz et al. (2009) for 29 nearby ($16 < r < 240$ pc), bright ($9.0 < V < 11.2$) *Kepler* targets which were observed photometrically by those authors. Molenda-Żakowicz et al. (2009) did not find any evidence that those stars were reddened while their $E(B-V)$ provided in the KIC were sometimes as high as 0.06 mag. The influence of the inaccurate $E(B-V)$ used by Pinsonneault et al. (2012) on the derived IRFM $T_{\rm eff}$ may be small but should be considered as one of possible sources of the scatter in the differences between $T_{\rm eff}$ derived from IRFM and from spectroscopy.

5.2 Metallicity

As shown in Fig. 2 *a*, *b*, and *c*, the values of [Fe/H] derived with ARES+MOOG, ROTFIT and VWA agree with each other to within the error bars for almost all targets. The mean differences between these determinations do not exceed 0.07 dex. Nevertheless, their standard deviation is quite large and equal to the typical uncertainty of the measurements obtained with ROTFIT, and twice as large as the uncertainties found with ARES+MOOG.

For the stars hotter than 6,000 K, [Fe/H] values computed with ARES+MOOG are slightly higher than those computed with ROTFIT or VWA (Fig. 2 *a* and *b*). However, this trend does not affect the overall consistency of the results. The [Fe/H] computed with ROTFIT and VWA agree best (Fig. 2 *c*) showing the mean difference of 0.03 dex and no trends at high temperatures. The high standard deviation is not reduced, though, and it is as high as that in Fig. 2 *a*, where the mean difference is the highest and the trend at the high temperatures, best visible.

5.3 Surface gravity

The surface gravity is the parameter which is least constrained when derived with ARES+MOOG. The reason for that is related to the number of iron lines used in this method. Although we use nearly 300 Fe I lines, which constrain very well the temperature, micro turbulence, and the metal abundance, $\log g$, which comes from the ionization balance, requires the analysis of the Fe II lines. Unfortunately the number of Fe II lines is limited to less than 20. Due to that small number, the results of their analysis are more sensitive to errors and more uncertain.

The differences between $\log g$ computed with ARES+MOOG, ROTFIT, and VWA (the spectroscopic $\log g$) illustrated in Fig. 3 *a* and *b*, are around 0.2 dex, and show the discrepancies increasing for the hot stars. The trends visible in Fig. 3 *a* and *b*, mimic those in Fig. 1 *a* and *b*, which may be a result of strong correlations between $T_{\rm eff}$ and $\log g$. The $\log g$ obtained with ROTFIT and with VWA agree with each other better (Fig. 3 *c*.) The mean difference between them is the lowest, 0.12 dex, and there are no trends for hot stars. Anyhow, the standard deviation of the differences is still high.

6 DISCUSSION

Our analysis shows that deriving precise and accurate atmospheric parameters is not an easy task. While within one method the precision of the computations can be high, when its results are compared to those obtained by means of other methods or from different data, various trends and offsets appear, proving that we are still far from being able to provide accurate $T_{\rm eff}$, $\log g$, and [Fe/H] for solar-type stars.

KIC 5184732 is a good example of those difficulties. In Table 2 we give the atmospheric parameters of that star derived independently from the spectra acquired with FRESCO, ESPaDOnS, and NARVAL. The atmospheric parameters computed with ARES+MOOG from the ESPaDOnS and NARVAL data agree with other nicely. The same can be said about the atmospheric parameters computed from those data with ROTFIT. However, the differences between those two sets of determinations amount to around 150 K in $T_{\rm eff}$, 0.12 dex in $\log g$, and 0.20 dex in [Fe/H]. For ROTFIT, there are also less pronounced but still not negligible differences between $T_{\rm eff}$, $\log g$ and [Fe/H] derived from the observations acquired with FRESCO and those obtained with ESPaDOnS and NARVAL.

The trends and discrepancies in the atmospheric parameters observed for stars hotter than 6,000 K are another significant but not a new problem. It has been thoroughly discussed, but not solved, by Torres et al. (2012). Those authors compare the atmospheric parameters obtained with SPC and SME, two codes in which the method of spectral synthesis is used, with $T_{\rm eff}$, $\log g$, and [Fe/H] computed with MOOG, that uses the curve-of-growth approach. The differences noticed by Torres et al. (2012) are the same as those reported in the present paper. The same trend can be noticed also in Fig. 3 *b*, in Sousa et al. (2008), where $T_{\rm eff}$ computed with ARES+MOOG are compared with those obtained with SME. The origin of those discrepancies is not clear but they seem to reflect real, systematic differences between the atmospheric parameters obtained from the spectral synthesis and the analysis of the equivalent widths. However, confirming that suspicion would require detailed examination of the input physics used in all the discussed methods which is beyond the scope of this paper.

The comparative analysis which we carried out in this paper showed that the accuracy of the atmospheric parameters of solar-type stars which is currently available is ± 150 K in $T_{\rm eff}$, ± 0.15 dex in [Fe/H] and ± 0.3 dex in $\log g$. That concerns particularly the faint stars and those hotter than 6,000 K. Since $\log g$ is the parameter most difficult to constraint in the spectroscopic analysis, for stars showing solar-like pulsations and those with transits, the seismic $\log g$ or those derived from the transit light curves may be used optionally as an alternative values. The former determinations of $\log g$ have been shown by Gai et al. (2011) to be nearly independent of the input physics used in different evolutionary models. The latter, deriving of which is described in detail by Seager & Mallen-Ornelas (2003), are currently preferred in the investigation of the transiting planets for which the spectroscopic $\log g$ are avoided (c.f. Torres et al. 2012).

7 SUMMARY

In this paper, we provided two determinations of the atmospheric parameters obtained for 169 stars, dwarfs and giants, with $T_{\rm eff}$ ranging from 3,200 to 6,700 K. The first set was computed with ARES+MOOG, a method which is based on the analysis of the equivalent widths of the spectral lines, the other, with ROTFIT, which makes use of the full target spectrum that is compared with a grid of reference star with well-known atmospheric parameters (mainly from spectral synthesis).

For 69 stars, $T_{\rm eff}$, $\log g$, [Fe/H], $v \sin i$, and the spectral type are provided for the first time in this paper.

KIC 9025370, KIC 9693187, and KIC 11179629 are newly discovered double-lined spectroscopic binary systems.

The internal precision of $T_{\rm eff}$ and [Fe/H] obtained with ARES+MOOG and ROTFIT is high, typically ± 80 K in $T_{\rm eff}$ (depending on the star; ARES+MOOG is slightly more precise than ROTFIT), ± 0.12 dex in $\log g$ for both methods, and ± 0.06 or ± 0.10 dex in [Fe/H] for ARES+MOOG and ROTFIT, respectively, as estimated from the standard deviations of the atmospheric parameters in Table 2. Therefore, our determinations can be safely used for the asteroseismic modelling of stars. However, we showed that for the solar-type stars the present accuracy of the determinations of the atmospheric parameters available in the literature is $T_{\rm eff}$ is $\pm$ 150 K, $\pm$ 0.15 dex in [Fe/H], and $\pm$ 0.3 dex in $\log g$.

Our results emphasise the importance of collecting high-quality spectra with sufficiently large telescopes equipped with performant spectrographs, and the need of examining the reasons why for the hot stars the spectral synthesis method and the curve-of-growth analysis yield the atmospheric parameters which are systematically different.

ACKNOWLEDGEMENTS

We thank Thierry Louge for help in retrieving the data from the CNRS/INSU CDAB/Bass2000 TBLegacy database operated by the University of Toulouse/OMP, Tarbes, France. We thank the Spanish Night time CAT for awarding the observing time to programs 61-Mercator3/11B, 119-NOT12/11A, and 61-NOT7/10A. J.M.-Ż., E.N., and D.D. acknowledge the Polish MNiSW grant N N203 405139. S.G.S., A.M., and M.T. acknowledge the support of the European Research Council/European Community under the FP7 through Starting Grant agreement number 239953. S.G.S. and J.M.-Ż. acknowledge the support from Fundação para a Ciência e a Tecnologia (FCT) through the grant SFRH/BPD/47611/2008, the projects PTDC/CTE-AST/098528/2008, PTDC/CTE-AST/098754/2008, and the 'Cooperação Cientifica e Tecnologica FCT/Polonia 2011/2012 (Proc. 441.00 Polonia)', funded by FCT/MCTES, Portugal and POPH/FSE (EC). SB acknowledges funding from the European Research Council under the European Community's Seventh Framework Programme (FP7/2007–2013)/ERC grant agreement n°227224 (PROSPERITY). M.B. is F.R.S.-FNRS Postdoctoral Researcher, Belgium.

REFERENCES

Borucki, W. J., Koch, D. G., Lissauer, J. J., et al. 2003, in Society of Photo-Optical Instrumentation Engineers (SPIE) Conference Series, Vol. 4854, Society of Photo-Optical Instrumentation Engineers (SPIE) Conference Series, ed. J.C. Blades & O.H.W. Siegmund, 129140

Brown, T.M., Latham, D.W., Everett, M.E., & Esquerdo, G.A. 2011, AJ, 142, 112

Bruntt, H., Basu, S., Smalley, B., Chaplin, W.J., Verner, G.A., et al. 2012, MNRAS 423, 122

Donati, J.-F., Semel, M., Carter, B.D., Rees, D.E., & Collier Cameron, A. 1997, MNRAS, 291, 658

Frasca, A., Alcalà, J. M., Covino, E., et al. 2003, A&A, 405, 149

Frasca, A., Guillout, P., Marilli, E., et al. 2006, A&A, 454, 301

Gai N., Basu S., Chaplin W. J., & Elsworth Y. 2011, ApJ, 730, 63

Guillout, P., Schmitt, J.H.M.M., Egret, D., Voges, W., Motch, C., & Sterzik, M.F. 1999, A&A 351, 1003

Hog E., Fabricius C., Makarov V.V., Urban S., Corbin T., Wycoff G., Bastian U., Schwekendiek P., & Wicenec A. 2000, A&A, 355, 27

Howell, S.B., Rowe, J.F., Bryson, S.T., Quinn, S.N., Marcy, G.W., et al. 2012, ApJ, 746, 123

Katz, D., Soubiran, C., Cayrel, R., Adda, M., & Cautain, R. 1998, A&A, 338, 151

Koch, D. G., Borucki, W. J., Basri, G., et al. 2010, ApJ, 713, L79

Kupka, F., Piskunov, N., Ryabchikova, T. A., Stempels, H. C., & Weiss, W. W. 1999, A&AS, 138, 119

Kurucz, R. 1993, ATLAS9 Stellar Atmosphere Programs and 2 km/s grid. Kurucz CD-ROM No. 13, Cambridge (Mass.: Smithsonian Astrophysical Observatory)

Molenda-Żakowicz, J., Frasca, A., Latham, D.W., & Jerzykiewicz, M. 2007, AcA, 57, 301

Molenda-Żakowicz, J., Kopacki, G., Stęślicki, M., & Narwid, A. 2009, AcA, 59, 193

Pinsonneault, M.H., An, D., Molenda-Żakowicz, J., Chap-

lin, W.J., Metcalfe, T.S., & Bruntt, H. 2012, ApJS 199, 30
Prugniel, Ph., & Soubiran, C. 2001, A&A, 369, 1048
Raskin, G., Van Winckel, H., Hensberge, H, et al. 2011, A&A, 526, 69
Santos, N. C., Israelian, G., & Mayor, M. 2004, A&A, 415, 1153
Seager, S. & Mallen-Ornelas, G. 2003, ApJ, 585, 1038
Sneden, C. 1973, Ph.D. Thesis, Univ. of Texas
Soubiran, C., Katz, D., & Cayrel, R. 1998, A&AS, 133, 221
Soubiran, C., Le Campion J.-F., Cayrel de Strobel G., & Caillo A. 2010 A&A 515, A111
Sousa, S.G., Santos, N.C., Israelian, G., Mayor, M., & Monteiro, M.J.P.F.G. 2006, A&A, 458, 873
Sousa, S.G., Santos, N.C., Israelian, G., Mayor, M., & Monteiro, M.J.P.F.G. 2007, A&A, 469, 783
Sousa, S.G., Santos, N.C., Israelian, G., Mayor, M., & Udry, S. 2011, A&A, 533, A141
Sousa, S.G., Santos, N.C., Israelian, G., et al. 2011a, A&A, 526, A99
Sousa, S.G., Santos, N.C., Israelian, G., Mayor, M., & Udry, S. 2011b, A&A, 533, A141
Sousa, S.G., Santos, N.C., Mayor, M., Udry, S., Casagrande, L., Israelian, G., Pepe, F., Queloz, D., & Monteiro, M.J.P.F.G. 2008, A&A, 487, 373
Stempels E. 2004, FIES Automatic Data Reduction Software, http://www.not.iac.es/instruments/fies/fiestool/FIEStool-manual-1.0.pdf
Thygesen, A.O., Frandsen, S., Bruntt, H., Kallinger, T., Andersen, M.F., et al. 2012, A&A, 543, A160
Torres, G., Fischer, D.A., Sozzetti, A., Buchhave, L.A., Winn, J.N., Holman, M.J., & Carter, J.A. 2012, ApJ, 757, 161
Uytterhoeven, K., Szabo, R., Southworth, J., et al. 2010a, AN, 331, P30 (arXiv:1003.6089)
Uytterhoeven, K., Briquet, M., Bruntt, H., et al. 2010b, AN, 331, 993

Table 2. The atmospheric parameters of the programme stars. In bold font, we indicate those stars for which the atmospheric parameters are derived for the first time.

KIC	ROTFIT $T_{\rm eff}$ [K]	σ	$\log g$ [cm s^{-2}]	σ	[Fe/H]	σ	$v \sin i$ [km s^{-1}]	σ	MK	ARES+MOOG $T_{\rm eff}$ [K]	σ	$\log g$ [cm s^{-2}]	σ	[Fe/H]	σ	$\xi_{\rm t}$ [km s^{-1}]	σ	Instrument
1430163	6412	99	3.97	0.10	−0.25	0.11	8.1	0.9	F5IV	6833	87	4.70	0.11	0.02	0.06	2.12	0.10	NARVAL
1435467	6169	108	3.95	0.11	−0.04	0.12	9.0	1.0	F8IV	6485	92	4.53	0.13	0.08	0.07	2.02	0.09	NARVAL
2837475	6462	102	3.95	0.13	−0.06	0.11	18.3	1.0	F5IV-V	—	—	—	—	—	—	—	—	ESPaDOnS
3335176	3225	110	1.23	1.24	−0.22	0.11	9.3	2.5	M7II	—	—	—	—	—	—	—	—	**FIES**
3424541	6165	80	3.90	0.10	0.13	0.11	24.6	0.8	G0IV	—	—	—	—	—	—	—	—	NARVAL
3427720	5949	66	4.26	0.11	0.00	0.11	2.0	0.7	F9IV-V	6111	68	4.51	0.11	0.04	0.06	1.25	0.04	ESPaDOnS
3430868	4969	71	2.91	0.13	−0.01	0.10	2.6	0.4	G8III	5208	67	3.24	0.12	0.13	0.06	1.46	0.03	ESPaDOnS
3443483	4856	58	3.05	0.11	0.04	0.10	11.1	0.2	K1IV	5043	82	3.43	0.18	0.09	0.06	1.63	0.06	**FIES**
3456181	6290	84	3.94	0.10	−0.24	0.10	5.0	1.0	F5IV-V	6584	91	4.43	0.11	-0.02	0.07	2.01	0.11	NARVAL
3632418	6148	84	3.94	0.11	−0.19	0.11	6.3	0.5	F6IV	6409	74	4.43	0.12	-0.03	0.06	1.86	0.06	NARVAL
3643774	5928	63	4.26	0.12	0.17	0.11	1.4	1.4	G2IV	6125	75	4.39	0.12	0.25	0.06	1.39	0.05	**HERMES**
3644223	4918	59	3.11	0.16	−0.22	0.11	2.8	0.8	G8III	—	—	—	—	—	—	—	—	**FRESCO**
3656476	5586	80	4.07	0.11	0.20	0.10	1.4	0.4	G5IV	5719	64	4.26	0.11	0.28	0.05	1.11	0.03	ESPaDOnS
3733735	6548	138	3.99	0.12	−0.12	0.11	13.0	1.4	F5IV-V	—	—	—	—	—	—	—	—	ESPaDOnS
3747220	6668	128	4.18	0.11	0.00	0.10	50.8	12.4	F3V	—	—	—	—	—	—	—	—	**ESPaDOnS**
4072740	4847	60	3.08	0.14	0.09	0.10	1.6	0.3	K1IV	4960	77	3.49	0.13	0.19	0.06	1.13	0.06	NARVAL
4346201	6154	81	3.98	0.12	−0.25	0.11	2.8	1.0	F8V	6239	91	4.28	0.12	-0.17	0.07	1.64	0.10	**HERMES**
4586099	6304	81	3.92	0.10	−0.20	0.11	2.3	0.7	F5IV-V	6533	80	4.37	0.11	-0.04	0.06	1.84	0.08	ESPaDOnS
4638884	6286	100	3.91	0.10	−0.17	0.11	4.6	0.8	F5IV-V	6684	98	4.58	0.17	-0.05	0.08	3.39	0.28	NARVAL
4859338	6013	109	4.09	0.13	0.19	0.11	34.3	1.5	G0IV	—	—	—	—	—	—	—	—	**HERMES**
4914923	5808	56	4.28	0.10	0.13	0.10	2.3	0.8	G1.5V	5948	65	4.34	0.12	0.18	0.05	1.26	0.03	ESPaDOnS
4931363	7045	106	4.07	0.12	−0.05	0.11	65.9	8.0	F0III	—	—	—	—	—	—	—	—	**ESPaDOnS**
4931390	6410	143	3.97	0.11	−0.25	0.11	3.2	1.2	F5IV-V	6862	80	4.55	0.11	-0.02	0.06	1.93	0.09	**ESPaDOnS**
5021689	6141	79	3.94	0.11	−0.16	0.12	7.0	0.6	F8IV	6378	80	4.55	0.13	-0.02	0.06	1.90	0.08	ESPaDOnS
5024851	4046	56	1.77	0.10	−0.18	0.10	1.9	0.7	K4III	—	—	—	—	—	—	—	—	**ESPaDOnS**
5080290	5157	153	3.60	0.30	−0.06	0.12	4.6	0.9	K0III-IV	5072	77	3.31	0.16	-0.10	0.07	0.69	0.07	**HERMES**
...	5261	167	4.21	0.18	0.01	0.13	6.1	0.5	K0III-IV	5064	78	3.28	0.13	-0.14	0.06	0.79	0.06	**ESPaDOnS**
5112786	4207	57	1.99	0.11	−0.17	0.10	2.5	0.9	K3III	4477	114	2.21	0.22	-0.13	0.07	1.83	0.08	**ESPaDOnS**
5184732	5669	65	4.07	0.11	0.24	0.10	2.8	0.3	G4V	—	—	—	—	—	—	—	—	**FRESCO**
...	5723	73	4.18	0.14	0.21	0.10	2.2	0.6	G4V	5894	68	4.31	0.12	0.43	0.06	1.18	0.03	ESPaDOnS*
...	5740	89	4.22	0.12	0.18	0.10	2.4	0.5	G1V	5877	68	4.34	0.11	0.40	0.06	1.14	0.03	NARVAL*
5199859	3722	112	1.63	0.30	−0.07	0.11	10.8	1.3	M0III	—	—	—	—	—	—	—	—	**FIES**
5371516	6138	54	3.98	0.12	0.10	0.10	9.7	1.2	F8IV	6526	107	4.49	0.15	0.11	0.08	2.35	0.14	ESPaDOnS
5450445	6099	68	4.13	0.11	0.05	0.11	5.4	0.6	F8V	6396	75	4.49	0.11	0.23	0.06	1.75	0.06	NARVAL
5512589	5764	61	4.22	0.11	0.06	0.11	1.6	0.4	G3V	5812	66	4.05	0.11	0.12	0.06	1.20	0.03	NARVAL
5557932	5936	69	4.37	0.11	0.00	0.10	13.7	0.3	G1.5V	—	—	—	—	—	—	—	—	**ESPaDOnS**
5596656	5375	86	3.99	0.16	−0.18	0.11	3.8	0.4	G5IV	5188	69	3.75	0.13	-0.44	0.06	1.05	0.05	ESPaDOnS
5620305	5190	129	3.49	0.26	−0.01	0.11	4.2	1.1	K0III-IV	5040	70	2.95	0.12	-0.01	0.06	0.51	0.05	**HERMES**
5701829	4927	74	3.19	0.12	−0.24	0.10	2.3	0.5	K0IV	—	—	—	—	—	—	—	—	**FRESCO**
...	4914	56	3.18	0.12	−0.13	0.11	2.4	0.7	K0IV	4962	69	3.39	0.13	-0.17	0.06	1.13	0.04	ESPaDOnS
5737655	5163	71	2.88	0.17	−0.44	0.11	3.8	0.6	G4III-IV	5121	63	2.83	0.10	-0.56	0.05	1.68	0.02	**ESPaDOnS**
5773345	6007	86	4.17	0.11	0.13	0.10	3.4	1.1	G0.5IV	6399	71	4.36	0.11	0.30	0.06	1.92	0.05	ESPaDOnS

Table 1. continuation.

KIC	$T_{\rm eff}$ [K]	σ	$\log g$ [cm s^{-2}]	σ	[Fe/H]	σ	$v \sin i$ [km s^{-1}]	σ	MK	$T_{\rm eff}$ [K]	σ	$\log g$ [cm s^{-2}]	σ	[Fe/H]	σ	$\xi_{\rm t}$ [km s^{-1}]	σ	Instrument
	ROTFIT									ARES+MOOG								
5774694	5804	55	4.34	0.10	0.08	0.10	3.6	0.5	G2V	5923	65	4.56	0.10	0.10	0.05	1.17	0.03	ESPaDOnS*
...	5801	66	4.34	0.11	0.06	0.10	3.6	0.6	G3V	5950	64	4.58	0.10	0.09	0.05	1.19	0.03	NARVAL*
5952403	5058	77	2.99	0.19	0.01	0.10	13.6	0.1	G8III	—	—	—	—	—	—	—	—	**FIES**
5955122	5952	69	4.13	0.11	−0.05	0.12	4.5	0.6	F9IV-V	6092	69	4.26	0.12	-0.06	0.06	1.66	0.05	ESPaDOnS
6116048	5991	101	4.09	0.12	−0.24	0.13	2.9	0.6	F9IV-V	6152	66	4.53	0.10	-0.14	0.05	1.36	0.04	ESPaDOnS
6225718	6138	78	3.96	0.11	−0.23	0.12	2.4	0.5	F8V	6366	70	4.61	0.11	-0.07	0.06	1.50	0.05	NARVAL
6285677	5849	64	4.32	0.12	0.06	0.12	7.6	1.0	G2V	6205	73	4.48	0.11	0.23	0.06	1.48	0.05	**HERMES**
...	5907	60	4.18	0.11	0.02	0.10	7.8	0.9	G0.5IV	—	—	—	—	—	—	—	—	**FRESCO**
6370489	6241	90	3.98	0.10	−0.35	0.11	4.4	0.8	F8V	—	—	—	—	—	—	—	—	**FIES**
6442183	5736	63	4.26	0.11	−0.07	0.11	1.7	0.5	G1V	5738	62	4.14	0.10	-0.12	0.05	1.15	0.02	NARVAL
6508366	6332	92	3.91	0.11	−0.07	0.11	18.0	1.0	F6IV	—	—	—	—	—	—	—	—	ESPaDOnS
6590668	4463	58	2.02	0.12	−0.22	0.10	4.0	1.1	K1IIII	—	—	—	—	—	—	—	—	**FRESCO**
6603624	5471	105	4.02	0.14	0.17	0.11	1.4	0.7	G8IV-V	5718	78	4.44	0.13	0.28	0.06	1.16	0.06	ESPaDOnS
6679371	6344	109	3.92	0.11	−0.10	0.11	11.0	1.0	F5IV-V	—	—	—	—	—	—	—	—	NARVAL
6766118	4892	58	2.73	0.10	0.05	0.10	2.7	0.6	K0III	—	—	—	—	—	—	—	—	**FRESCO**
6933899	5837	65	4.21	0.12	0.04	0.10	2.0	0.6	G0.5IV	5921	65	4.12	0.11	0.04	0.06	1.29	0.03	NARVAL
7103006	6180	96	3.92	0.11	−0.07	0.12	8.9	0.6	F8IV	6685	86	4.50	0.11	0.19	0.06	1.98	0.08	NARVAL
7206837	6142	85	4.05	0.11	0.05	0.11	6.7	0.5	F8IV	6573	80	4.61	0.11	0.22	0.06	1.93	0.06	NARVAL
7282890	6207	64	3.89	0.12	0.02	0.11	21.0	1.0	F6IV	—	—	—	—	—	—	—	—	ESPaDOnS
7510397	6120	64	3.94	0.11	−0.26	0.12	2.2	0.8	F6IV	6362	80	4.54	0.12	-0.08	0.06	1.66	0.07	ESPaDOnS
7529180	6470	106	4.03	0.11	−0.06	0.11	27.0	1.7	F5IV-V	—	—	—	—	—	—	—	—	NARVAL
7662428	6143	64	4.03	0.11	0.10	0.10	9.3	0.8	F8V	6504	141	4.93	0.19	-0.09	0.10	1.58	0.22	ESPaDOnS
7668623	6159	76	3.94	0.11	−0.10	0.13	7.6	0.7	F8IV	6580	112	4.56	0.15	0.03	0.08	2.54	0.21	ESPaDOnS
7680114	5799	55	4.25	0.11	0.08	0.10	1.4	0.8	G0V	5955	68	4.41	0.11	0.12	0.06	1.30	0.04	NARVAL
7730305	6060	74	4.25	0.12	0.09	0.11	12.6	1.1	F8V	6304	81	4.67	0.11	0.17	0.06	1.69	0.07	**HERMES**
...	6030	75	4.17	0.10	0.01	0.11	15.0	0.8	F8V	—	—	—	—	—	—	—	—	**FRESCO**
7747078	5994	87	4.04	0.13	−0.19	0.13	3.8	0.8	F9IV-V	6114	78	4.37	0.12	-0.11	0.06	1.65	0.07	ESPaDOnS
7799349	4954	57	3.33	0.12	0.14	0.10	1.1	0.4	K1IV	5175	84	3.81	0.15	0.24	0.07	1.31	0.07	NARVAL
7799575	3941	56	1.69	0.10	−0.17	0.10	2.2	0.7	K5III	—	—	—	—	—	—	—	—	**ESPaDOnS**
7800289	6398	112	3.96	0.11	−0.17	0.10	18.6	1.1	F5IV	—	—	—	—	—	—	—	—	NARVAL
7871531	5498	92	4.31	0.10	−0.12	0.11	2.2	0.8	G5V	5461	67	4.40	0.12	-0.26	0.06	0.87	0.05	ESPaDOnS
7940546	6243	70	3.92	0.10	−0.25	0.10	6.6	0.8	F6IV	6427	82	4.52	0.12	-0.11	0.06	2.09	0.09	ESPaDOnS*
...	6226	94	3.94	0.10	−0.24	0.11	7.0	0.7	F6IV	6472	84	4.59	0.12	-0.11	0.06	2.32	0.12	NARVAL*
7970740	5354	84	4.36	0.11	−0.31	0.11	2.4	0.5	G9V	5287	68	4.49	0.11	-0.52	0.05	0.59	0.08	ESPaDOnS
7976303	6119	77	3.97	0.10	−0.38	0.10	3.1	0.5	F8V	6203	76	4.15	0.11	-0.41	0.06	1.62	0.07	ESPaDOnS
7985370	5836	73	4.39	0.11	0.02	0.11	16.4	0.3	G1.5V	—	—	—	—	—	—	—	—	**HERMES**
...	5849	54	4.28	0.11	−0.10	0.11	17.3	0.4	G1.5V	—	—	—	—	—	—	—	—	**FRESCO**
8006161	5258	65	4.13	0.17	0.23	0.11	2.0	0.5	G8V	5431	82	4.45	0.13	0.30	0.06	0.95	0.10	ESPaDOnS*
...	5211	71	4.05	0.16	0.20	0.11	1.9	0.3	G8V	5468	77	4.41	0.13	0.29	0.06	1.07	0.07	NARVAL*
8026226	6276	60	3.90	0.10	−0.20	0.11	7.4	0.5	F5IV-V	6469	78	4.32	0.13	-0.13	0.06	2.72	0.18	ESPaDOnS
8179536	6160	86	3.98	0.11	−0.16	0.11	8.1	0.6	F6IV	6536	74	4.64	0.11	0.13	0.06	1.61	0.05	NARVAL

Table 1. continuation.

KIC	$T_{\rm eff}$ [K]	σ	$\log g$ [cm s^{-2}]	σ	[Fe/H]	σ	$v \sin i$ [km s^{-1}]	σ	MK	$T_{\rm eff}$ [K]	σ	$\log g$ [cm s^{-2}]	σ	[Fe/H]	σ	$\xi_{\rm t}$ [km s^{-1}]	σ	Instrument
	ROTFIT									ARES+MOOG								
8211551	4812	59	2.83	0.13	−0.12	0.10	1.9	0.5	G9III	4882	68	2.76	0.12	-0.15	0.06	1.54	0.03	ESPaDOnS*
...	4820	59	2.83	0.12	−0.10	0.10	2.0	0.3	G9III	4887	70	2.69	0.13	-0.17	0.06	1.56	0.03	NARVAL*
8228742	6061	80	4.02	0.12	−0.12	0.11	3.3	1.1	F9IV-V	6295	76	4.42	0.11	0.00	0.06	1.71	0.06	ESPaDOnS
8343931	6506	102	4.09	0.12	−0.03	0.10	43.2	4.0	F5IV-V	—	—	—	—	—	—	—	—	**ESPaDOnS**
8346342	6141	94	3.93	0.11	−0.05	0.12	6.9	0.8	F8IV	6573	139	4.59	0.12	0.21	0.10	1.87	0.15	**ESPaDOnS**
8352528	3972	51	1.69	0.11	−0.18	0.10	2.2	0.9	K5III	—	—	—	—	—	—	—	—	**ESPaDOnS**
8360349	6176	55	3.92	0.11	0.07	0.10	10.6	0.7	F8IV	6762	156	4.92	0.15	0.07	0.10	3.45	0.37	ESPaDOnS
8367710	6227	90	3.92	0.10	0.02	0.11	15.0	1.1	F6IV	—	—	—	—	—	—	—	—	ESPaDOnS
8379927	5998	80	4.25	0.11	−0.03	0.12	8.8	0.8	F9IV-V	6225	95	4.76	0.13	-0.23	0.07	2.01	0.13	ESPaDOnS*
...	6000	86	4.12	0.12	−0.05	0.13	13.0	2.0	F9IV-V	6202	73	4.47	0.12	-0.20	0.06	0.95	0.05	NARVAL*
8394589	6111	90	3.98	0.11	−0.37	0.11	4.4	0.8	F8V	6231	75	4.54	0.11	-0.24	0.06	1.36	0.07	NARVAL
8429280	5029	73	4.35	0.10	−0.04	0.11	34.8	0.6	K2V	—	—	—	—	—	—	—	—	**FRESCO**
...	5108	88	4.56	0.13	0.06	0.11	33.2	1.0	K1V	—	—	—	—	—	—	—	—	**HERMES**
8491147	5007	61	2.92	0.15	−0.24	0.11	2.5	0.6	G8III	5065	65	2.75	0.12	-0.31	0.06	1.57	0.02	ESPaDOnS
8524425	5671	76	4.17	0.12	0.12	0.11	1.1	0.5	G2.5V	5664	65	4.09	0.11	0.13	0.05	1.16	0.03	NARVAL
8542853	5594	68	4.34	0.10	−0.09	0.11	2.1	0.6	G6V	5580	68	4.54	0.12	-0.20	0.06	0.85	0.06	ESPaDOnS
8547390	4732	53	2.80	0.11	−0.01	0.10	3.0	0.3	K0III	4870	74	2.86	0.15	0.12	0.06	1.60	0.04	ESPaDOnS
8561221	5290	89	3.76	0.13	−0.04	0.10	1.9	0.6	G9.5IV	5352	68	3.80	0.11	-0.04	0.06	1.14	0.04	NARVAL
8579578	6297	125	3.91	0.11	−0.06	0.11	19.3	1.0	F6IV	—	—	—	—	—	—	—	—	NARVAL
8677933	5946	144	3.92	0.23	0.15	0.12	49.6	0.7	G0IV	—	—	—	—	—	—	—	—	**ESPaDOnS**
8694723	6258	92	3.97	0.11	−0.42	0.11	4.6	1.0	G0IV	6445	80	4.55	0.11	-0.39	0.06	1.91	0.11	NARVAL
...	6287	90	4.00	0.10	−0.38	0.12	3.8	0.7	G0IV	6489	85	4.50	0.13	-0.35	0.06	1.98	0.13	**FIES**
8702606	5621	78	4.08	0.11	0.00	0.11	0.7	0.7	G5IV-V	5578	62	3.89	0.10	-0.06	0.05	1.16	0.02	ESPaDOnS
8738809	6039	74	4.19	0.11	0.07	0.11	2.2	0.9	G0.5IV	6207	68	4.17	0.11	0.12	0.06	1.65	0.03	NARVAL
8751420	5281	89	3.86	0.16	−0.11	0.11	1.1	0.5	G8IV	5330	62	3.84	0.10	-0.14	0.05	1.07	0.02	NARVAL
8760414	5850	149	3.94	0.19	−0.90	0.22	3.4	2.3	G0IV	5924	77	4.53	0.11	-1.00	0.06	1.38	0.11	NARVAL
8816903	7063	122	4.12	0.10	−0.05	0.10	57.6	5.0	F0V	—	—	—	—	—	—	—	—	**ESPaDOnS**
8831759	3877	79	1.66	0.16	−0.11	0.10	2.4	0.7	M1III	4920	209	3.94	0.34	-0.14	0.10	3.65	0.58	**ESPaDOnS**
8866102	6195	113	3.95	0.10	−0.16	0.11	11.0	0.8	F6IV	—	—	—	—	—	—	—	—	**ESPaDOnS**
8938364	5702	70	4.25	0.11	−0.16	0.12	2.0	0.9	G3V	5808	71	4.31	0.12	-0.10	0.06	1.10	0.05	NARVAL
9098294	5766	63	4.27	0.10	−0.22	0.12	2.6	0.6	G3V	5959	80	4.56	0.12	-0.04	0.06	1.13	0.07	NARVAL
9116461	6358	80	3.95	0.10	−0.14	0.11	14.1	0.6	F5IV-V	—	—	—	—	—	—	—	—	**ESPaDOnS**
9139151	6004	60	4.26	0.10	0.07	0.10	3.2	0.5	G0.5IV	6213	67	4.64	0.11	0.17	0.06	1.24	0.04	ESPaDOnS
9139163	6175	100	3.99	0.12	0.00	0.11	2.0	1.0	F8IV	6577	69	4.44	0.10	0.21	0.06	1.68	0.04	ESPaDOnS*
...	6151	106	3.98	0.11	−0.05	0.12	1.9	0.8	F8IV	6584	67	4.47	0.11	0.19	0.05	1.70	0.03	NARVAL*
9206432	6204	122	3.95	0.11	−0.02	0.12	1.7	1.2	F8IV	6772	73	4.61	0.11	0.28	0.06	1.92	0.05	ESPaDOnS
9226926	6580	122	4.12	0.11	−0.15	0.12	30.8	3.0	F5V	—	—	—	—	—	—	—	—	NARVAL
9289275	5931	73	4.25	0.12	0.07	0.12	2.7	1.5	G0.5IV	6208	77	4.40	0.12	0.20	0.06	1.51	0.06	**HERMES**
9414417	6242	74	3.92	0.10	−0.19	0.11	6.0	1.1	F6IV	6496	124	4.66	0.13	-0.07	0.09	2.55	0.26	**HERMES**
9512063	5882	85	4.14	0.12	−0.19	0.16	2.5	1.3	F9IV-V	5842	72	3.87	0.11	-0.15	0.06	1.12	0.04	**HERMES**
9514879	5971	57	4.31	0.11	0.02	0.10	10.1	0.3	G1.5V	6190	79	4.70	0.12	0.12	0.06	1.60	0.07	**FIES**
9532030	4472	56	2.35	0.12	−0.11	0.10	3.6	0.5	G9III	4596	85	2.53	0.17	-0.06	0.06	1.74	0.06	ESPaDOnS
9534041	5061	63	3.10	0.14	0.02	0.10	3.2	0.6	G8III	5278	72	3.28	0.12	-0.01	0.06	1.49	0.04	**ESPaDOnS**

Table 1. continuation.

KIC	$T_{\rm eff}$ [K]	σ	$\log g$ [cm s^{-2}]	σ	[Fe/H]	σ	$v \sin i$ [km s^{-1}]	σ	MK	$T_{\rm eff}$ [K]	σ	$\log g$ [cm s^{-2}]	σ	[Fe/H]	σ	$\xi_{\rm t}$ [km s^{-1}]	σ	Instrument
	ROTFIT									ARES+MOOG								
9605196	4455	54	1.91	0.14	−0.20	0.11	3.5	0.8	K1III	—	—	—	—	—	—	—	—	**FRESCO**
9655101	5039	107	3.02	0.18	0.00	0.11	3.5	0.7	G8III	5227	73	3.31	0.13	-0.02	0.06	1.53	0.04	**ESPaDOnS**
9655167	5036	82	3.03	0.17	−0.01	0.10	4.5	0.5	G8III	5325	80	3.57	0.15	0.06	0.07	1.57	0.06	**ESPaDOnS**
9700679	5176	140	3.37	0.26	0.04	0.12	3.7	0.9	G8III	5101	73	3.05	0.13	-0.08	0.06	1.01	0.04	**HERMES**
9702369	5956	110	4.04	0.12	−0.11	0.13	5.1	1.4	F9IV-V	6441	78	4.54	0.11	0.14	0.06	1.39	0.05	**HERMES**
9715099	6180	58	4.07	0.11	0.07	0.12	25.1	1.2	F6IV	—	—	—	—	—	—	—	—	**FRESCO**
9716090	5053	78	3.17	0.15	0.02	0.10	3.3	0.6	G8III	5297	74	3.41	0.12	-0.04	0.06	1.75	0.05	**ESPaDOnS**
9716522	4860	57	2.82	0.11	−0.03	0.10	2.7	0.3	G9III	5126	73	3.10	0.12	0.05	0.06	1.67	0.04	**ESPaDOnS**
9812850	6258	64	3.94	0.10	−0.22	0.11	9.8	0.7	F6IV	6790	118	4.92	0.13	-0.04	0.08	2.70	0.27	ESPaDOnS
9908400	6068	78	3.95	0.12	0.17	0.10	17.9	0.9	G0IV	—	—	—	—	—	—	—	—	NARVAL
9955598	5264	62	4.29	0.12	−0.04	0.11	1.2	0.6	K0V	5380	68	4.33	0.12	0.04	0.06	0.80	0.06	NARVAL
9965715	6326	91	4.00	0.10	−0.30	0.11	8.2	0.7	F2V	6542	87	4.71	0.12	-0.22	0.06	1.84	0.10	**ESPaDOnS**
10001154	4391	63	2.17	0.12	−0.23	0.10	2.6	0.2	G9III	4585	82	2.34	0.16	-0.20	0.06	2.06	0.06	**ESPaDOnS**
10010623	6464	77	4.11	0.11	−0.01	0.10	31.8	2.1	F3V	—	—	—	—	—	—	—	—	**ESPaDOnS**
10016239	6214	73	3.95	0.11	−0.17	0.11	10.7	1.0	F6IV	—	—	—	—	—	—	—	—	NARVAL
10018963	6145	86	3.95	0.10	−0.27	0.10	2.1	0.6	F6IV	6354	69	4.32	0.11	-0.16	0.05	1.79	0.05	NARVAL
10068307	6144	82	3.94	0.11	−0.22	0.11	3.4	0.8	F6IV	6288	68	4.28	0.10	-0.11	0.06	1.68	0.04	ESPaDOnS
10079226	5854	65	4.27	0.11	0.10	0.11	1.6	1.2	G0V	6045	68	4.49	0.11	0.17	0.06	1.17	0.04	**HERMES**
10124866	5736	56	4.29	0.11	−0.31	0.11	3.0	0.6	G4V	5864	68	4.57	0.11	-0.24	0.06	1.03	0.05	ESPaDOnS
10131030	4897	52	2.74	0.10	0.02	0.11	3.0	0.9	G8III	—	—	—	—	—	—	—	—	**FRESCO**
10162436	6149	89	3.95	0.11	−0.16	0.12	2.8	0.8	F8IV	6423	71	4.43	0.11	0.01	0.06	1.75	0.05	ESPaDOnS
10355856	6351	93	3.93	0.10	−0.22	0.11	4.5	0.8	F5IV-V	6612	79	4.38	0.11	-0.01	0.06	1.84	0.05	ESPaDOnS
10388249	4743	57	2.87	0.12	0.00	0.10	10.6	0.2	K1IV	4978	98	3.48	0.19	0.14	0.07	1.87	0.09	**FIES**
10454113	6129	133	4.07	0.12	−0.16	0.12	3.7	1.0	F9IV-V	6216	68	4.46	0.10	0.00	0.05	1.30	0.04	ESPaDOnS
10462940	6026	71	4.24	0.10	0.05	0.11	1.9	0.7	G0.5IV	6268	68	4.48	0.10	0.18	0.05	1.35	0.03	NARVAL
10516096	5928	62	4.24	0.11	−0.04	0.11	2.8	0.6	F9IV-V	6094	70	4.47	0.11	-0.03	0.06	1.39	0.05	ESPaDOnS
10526137	3316	264	3.93	0.54	−0.23	0.11	13.4	1.6	M2V	—	—	—	—	—	—	—	—	**FIES**
10644253	5910	58	4.30	0.10	0.05	0.10	1.6	0.7	G0V	6132	65	4.54	0.11	0.15	0.05	1.21	0.03	ESPaDOnS
10709834	6398	101	3.94	0.10	−0.20	0.11	7.0	1.2	F5IV-V	—	—	—	—	—	—	—	—	NARVAL
10735274	3836	189	1.72	0.31	−0.06	0.12	2.8	1.5	K5III	—	—	—	—	—	—	—	—	**HERMES**
...	4033	68	1.69	0.14	−0.17	0.08	9.3	2.0	K4III	—	—	—	—	—	—	—	—	**FRESCO**
10923629	6109	67	4.00	0.11	0.08	0.11	7.3	0.8	F8V	—	—	—	—	—	—	—	—	NARVAL
10963065	6097	108	4.00	0.11	−0.27	0.12	2.3	0.6	F8V	6236	64	4.55	0.11	-0.15	0.05	1.47	0.03	NARVAL
11018874	6454	97	4.08	0.11	−0.04	0.11	49.0	2.3	F5V	—	—	—	—	—	—	—	—	**ESPaDOnS**
11026764	5771	65	4.22	0.11	0.10	0.10	2.6	0.9	G1V	5802	68	4.12	0.11	0.11	0.06	1.30	0.04	ESPaDOnS
11037105	6801	110	4.20	0.12	−0.14	0.13	27.9	2.0	F2V	—	—	—	—	—	—	—	—	**ESPaDOnS**
11081729	6400	104	3.97	0.10	−0.19	0.12	21.4	0.7	F5IV	—	—	—	—	—	—	—	—	ESPaDOnS
11099165	3930	53	1.69	0.11	−0.18	0.10	2.5	0.7	K5III	—	—	—	—	—	—	—	—	**ESPaDOnS**
11137075	5576	68	4.14	0.12	−0.04	0.11	2.3	0.4	G5IV-V	5610	71	4.10	0.12	-0.06	0.06	1.10	0.04	NARVAL
11244118	5605	75	4.05	0.14	0.19	0.10	1.7	0.5	G5IV	5770	67	4.14	0.11	0.35	0.06	1.19	0.03	NARVAL
11253226	6410	102	3.96	0.11	−0.20	0.11	11.4	1.2	F5IV-V	—	—	—	—	—	—	—	—	ESPaDOnS
11342410	5858	83	4.26	0.11	−0.07	0.12	1.8	0.6	G1V	—	—	—	—	—	—	—	—	**FRESCO**

Table 1. continuation.

KIC	$T_{\rm eff}$ [K]	σ	$\log g$ [cm s^{-2}]	σ	[Fe/H]	σ	$v \sin i$ [km s^{-1}]	σ	MK	$T_{\rm eff}$ [K]	σ	$\log g$ [cm s^{-2}]	σ	[Fe/H]	σ	$\xi_{\rm t}$ [km s^{-1}]	σ	Instrument
	ROTFIT									ARES+MOOG								
11396108	6330	153	3.97	0.12	−0.03	0.11	20.1	1.9	F6IV	—	—	—	—	—	—	—	—	**FRESCO**
11414712	5731	58	4.16	0.11	0.02	0.10	2.3	0.9	G3V	5725	61	3.99	0.10	-0.02	0.05	1.27	0.01	NARVAL
11495120	4864	54	2.70	0.10	−0.09	0.11	2.9	0.5	G8III	—	—	—	—	—	—	—	—	**FRESCO**
11498538	6453	100	4.07	0.12	−0.01	0.10	33.2	1.3	F2V	—	—	—	—	—	—	—	—	ESPaDOnS
11551430	5649	121	4.01	0.12	−0.07	0.12	24.3	0.5	G5IV	—	—	—	—	—	—	—	—	**FRESCO**
11559263	5633	159	4.02	0.18	0.08	0.11	5.3	0.6	G5III	5284	66	3.03	0.11	-0.02	0.06	0.77	0.03	**HERMES**
11708170	6872	101	4.21	0.12	−0.04	0.10	32.9	2.3	F1V	—	—	—	—	—	—	—	—	**ESPaDOnS**
11709006	5852	75	4.38	0.10	0.01	0.11	10.2	0.2	G1.5V	6047	79	4.66	0.11	0.05	0.06	1.40	0.07	**HERMES**
11717120	5155	74	3.76	0.20	−0.17	0.11	0.6	0.3	G9.5IV	5118	67	3.80	0.12	-0.27	0.06	0.89	0.04	**FIES**
...	5222	82	3.82	0.16	−0.17	0.10	1.1	0.4	G8IV	5137	65	3.87	0.12	-0.28	0.05	0.83	0.04	NARVAL
11754082	4742	60	2.77	0.13	−0.10	0.10	11.5	2.7	G9III	—	—	—	—	—	—	—	—	**FRESCO**
11772920	5209	97	4.34	0.14	−0.07	0.10	1.4	0.8	K1V	5341	80	4.44	0.13	-0.10	0.06	0.73	0.10	**HERMES**
12009504	6099	102	4.00	0.11	−0.14	0.12	5.9	0.7	F9IV-V	6267	71	4.37	0.11	-0.03	0.06	1.59	0.06	ESPaDOnS
12155015	3937	55	1.68	0.11	−0.16	0.10	2.8	0.9	K5III	—	—	—	—	—	—	—	—	**ESPaDOnS**
12258514	5952	60	4.23	0.11	0.06	0.10	1.7	0.6	G0.5IV	6099	66	4.32	0.10	0.10	0.05	1.36	0.03	ESPaDOnS
12453925	6514	135	4.14	0.12	−0.02	0.10	75.2	2.9	F3V	—	—	—	—	—	—	—	—	**ESPaDOnS**
12455203	4919	59	2.89	0.12	−0.02	0.10	2.3	0.3	G8III	5104	69	3.14	0.13	0.07	0.06	1.49	0.03	ESPaDOnS
12508433	5134	97	3.50	0.21	0.08	0.12	0.6	0.4	K0III-IV	5281	76	3.85	0.13	0.21	0.06	0.98	0.06	**HERMES**

* We use an asterisk to indicate stars listed by Bruntt et al. (2012) or Thygesen et al. (2012) who do not provide the information whether they used the ESPaDOnS or the NARVAL spectraspectra in their analysis.